JOURNAL OF GEOPHYSICAL RESEARCH, VOL. 106, NO. A6, PAGES 10,565–10,579, JUNE 1, 2001

Current-induced magnetic field effects on bare tether current collection: A parametric study

G. V. Khazanov,[1] N. H. Stone,[2] E. N. Krivorutsky,[1] K. V. Gamayunov,[1] and M. W. Liemohn[3]

Abstract. The physical process of current collection by a "bare wire" electrodynamic tether in space is considered. The study uses an improved model that takes into account the resistance of the wire and the magnetic shielding induced by current flow in the tether. The plasma density, n_e, electron temperature, T_e, tether length, L, tether radius, r_w, and the angle of the geomagnetic field to the tether (90°-α) were all used as parameters. It is shown, for certain tether configurations and parameter values, that magnetic shielding reduces the collected current. In general, any parametric change that increases tether current, and hence, the strength of the current-induced magnetic field relative to the strength of the electric field between the tether and the ambient plasma, will increase the shielding effect. Tether current is increased directly with tether collection area (which depends on L and r_w), plasma conductivity (which depends on n_e and T_e), and the motional emf along the tether (which increases with L and the angle 90°-α). It turns out that, as any of these parameters change so as to cause the overall tether current to increase, the overestimate of current that results from ignoring the magnetic shielding effect becomes correspondingly greater. Moreover, it is shown that a tether system in the thruster (or motor) mode suffers greater current reduction from magnetic shielding than does the same tether deployed in the generator mode. Finally, it is shown that, for certain tether system configurations combined with particular values of the governing plasma parameters, current-induced magnetic shielding can significantly reduce the collected current and, therefore, system efficiency. For example, in the case of an electrodynamic tether system in the thruster mode under conditions of n_e=1.67x10^6 cm^{-3}, α=60°, r_w=2.5 mm, and E_m=34 V/km, magnetic shielding will reduce the collected current 10% at a point L=0.65 km along the tether (4.3 A instead of 4.8 A) and this increases to more than 40% at L=1.3km (9.6 A instead of 13.4 A).

1. Introduction

The concept of a long gravity-gradient-stabilized electrodynamic tether, serving as an energy transducer to convert spacecraft orbital energy to electrical power (or vice versa), has been the subject of intense theoretical and experimental investigations for some 20 years. The dozen or so missions flown to date demonstrate that space tethers are safe, easily deployed and controlled, and dynamically stable. Moreover, the TSS-1R mission has shown that electrodynamic tethers are capable of generating kilowatt levels of electrical power and thrust.

During the past few years, special attention has been given to the concept of a "bare" tether, proposed by *Sanmartin et al.* [1993], which uses the uninsulated tether wire as the positive electrode. A bare tether system will be flight tested for the first time in mid-2001 by NASA's Propulsive Small Expendable Deployer System (ProSEDS) mission. The existing electrodynamic models of bare tethers are based on the orbital motion limited (OML) theory of cylinder probes [*Laframboise,* 1966]. Such an approach to the description of current collection in a magnetized plasma is valid as long as the collected current is small and the wire radius is small compared to both the electron gyroradius and the thickness of the plasma sheath [*Laframboise and Rubinstein*, 1976; *Szuszczewicz and Takacs*, 1979; *Sanmartin and Estes,* 1999]. These requirements can be satisfied in Earth's ionospheric plasma with reasonable size limits on the tether radius (e.g., the most stringent condition is on the order of a few millimeters at 300 km altitude).

It is implicitly assumed in the OML model that the magnetic field induced by the tether current is negligibly small. However, the goal of achieving ever-increasing currents is a trait of the development of tether systems. As a result, the current-induced magnetic field can be larger than the Earth's magnetic field in a region comparable to other characteristic lengths of the system, such as the Debye radius or even the electron gyroradius. Perhaps more important than these effects, however, is the fact that the current-induced magnetic field completely changes the overall magnetic field topology around the tether [*Khazanov et al.,* 2000]. A closed, azimuthal magnetic field is produced around the tether by the tether current. As a result, the region immediately surrounding the tether is disconnected from the open magnetic field region farther out (a magnetic separatrix exists). Therefore, in order to be collected, charged particles must intersect the boundary surface (the separatrix) between the regions of closed and open magnetic fields. If the electric field outside the separatrix is weak compared to the electron thermal energy, then the tether is magnetically insu-

[1]Geophysical Institute, University of Alaska, Fairbanks, Alaska.
[2]Space Sciences Laboratory, NASA Marshall Space Flight Center, Huntsville, Alabama.
[3]Space Physics Research Laboratory, University of Michigan, Ann Arbor, Michigan.

Paper number 2000JA000345.
0148-0227/01/2000JA000345$09.00

lated and the current collected by the tether will be reduced to the level supported by electron diffusion across magnetic field lines (assuming end effects can be neglected). On the other hand, if the electric field outside the separatrix is strong enough, the tether will not be magnetically shielded and it can be assumed that the OML model applies.

To demonstrate the possible impact of this effect on current collection, a simple model was developed. *Khazanov et al.* [2000] assumed that the OML model could be used to calculate the current collected along the tether as long as the region of strong electric field extends beyond the region of closed magnetic surfaces. If the region of strong electric field was totally contained within the region of closed magnetic surfaces (by at least a Larmor radius inside the separatrix), it was assumed that electrons could not reach the wire and no current would be collected. It was found [*Khazanov et al.,* 2000] that for a long tether in a dense plasma, the current–induced magnetic field can significantly restrict current collected by the tether. The average inhomogeneity of the magnetic field near the wire was taken into account in the Larmor radius calculation. However, the resistivity of the tether was set to zero in this earlier model.

In the present study, we develop a more accurate model that relaxes some of the constraints of the earlier calculations and discuss the effect of current-induced magnetic shielding on bare tether current collection under more realistic conditions. This model takes into account tether resistivity and uses a more accurate calculation of electron flux in the region near the tether. The improved model also permits the analysis of the effect of weaker currents, such as those expected for the ProSEDS mission. Our main purposes in this paper are: (1) to demonstrate that, with the more accurate treatment, the current-induced magnetic field can still have a significant impact on tether current collection, and (2) to analyze the dependence of this effect on the tether system characteristics and ambient plasma parameters. Specific configurations that correspond to operational regimes expected for the ProSEDS tether system are used in the calculations.

In the next section the system of equations, used by *Sanmartin et al.* [1993] to describe the current and potential profiles along a bare tether, is generalized to take into account the effect of the current-induced azimuthal magnetic field on the flow of electrons into the region of current collection (i.e., the region within the separatrix). This set of generalized equations is then assimilated into our model. The code description is presented in section 3. The numerical results are presented and discussed in section 4, followed by a summary. The reduction in current collected at a fixed position along a segment of the tether where magnetic shielding is effective (where strong electric field is constrained to exist only inside the separatrix) is calculated in Appendix A.

2. Model of Current Collection Along the Tether

This section is based on the results presented by *Sanmartin et al.* [1993] and *Khazanov et al.* [2000], and so we follow the notations in these papers. As was noted above, the total magnetic field around the tether consists of the superposition of the Earth's magnetic field and the one induced by the tether current. If the tether current, **I**, is taken to be along the z axis and the external magnetic field, $\mathbf{B}_o$, to be in the y-z plane (see Figure 1a), the total magnetic field B can be written as

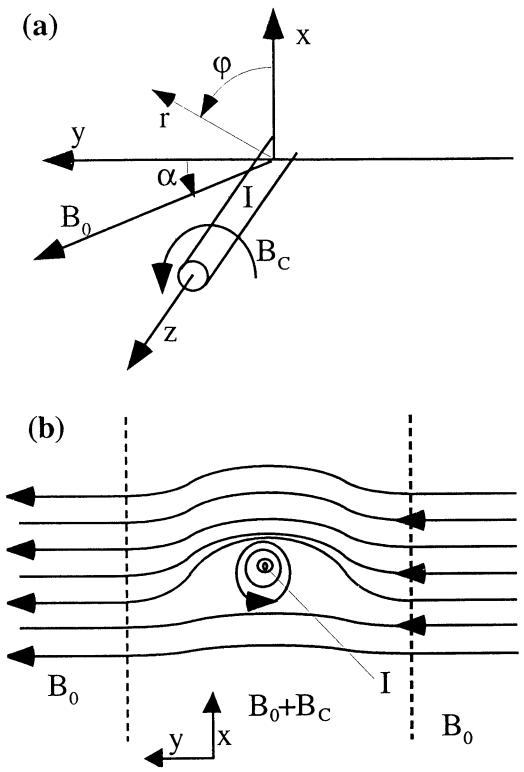

Figure 1. (a) Schematic of the relationship of the coordinate system to the current, ambient magnetic field, and induced magnetic field. (b) Schematic of the magnetic field topology around the wire, showing that the field is significantly modified by the current in a region near the wire (α=0).

$$\mathbf{B}=\mathbf{e}_r B_o\cos\alpha\sin\varphi+\mathbf{e}_\varphi\left[B_o\cos\alpha\cos\varphi+B_c\right]+\mathbf{e}_z B_o\sin\alpha\,, \tag{1}$$

where

$$B_c=\frac{2I}{cr}$$

and c is the velocity of light, polar coordinates r,φ in the x-y plane are introduced, $\mathbf{B}_c$ is the current-induced magnetic field, and α is the angle between the external magnetic field $\mathbf{B}_o$ and the x-y plane, that is, the complement of the angle between the tether and $\mathbf{B}_o$. Figure 1b shows a schematic of the magnetic field lines in the x-y plane. The field changes from its unperturbed state, $\mathbf{B}_o$, away from the tether to a mixture of $\mathbf{B}_o$ and $\mathbf{B}_c$ near the tether. The actual projections of the magnetic lines for such a field in the x-y plane are described by the expression

$$\xi=r^*\ln\frac{r}{r^*}+r\cos\alpha\cos\varphi=\text{const}\,, \tag{2}$$

where

$$r^*=\frac{2I}{cB_o}\,,$$

and are presented in Figure 2a in normalized units. A separatrix, marked as the dotted line $\xi_s=-r^*(1+\ln\cos\alpha)$, is the x-y plane projection of the magnetic field lines wound about the cylinder that divides the closed magnetic surfaces around the wire and the open surfaces farther out. Therefore the magnetic field lines near the wire are disconnected from infinity in the x-y plane. Also labeled in Figure 2a are the relative values of ξ for each region with respect to the separatrix.

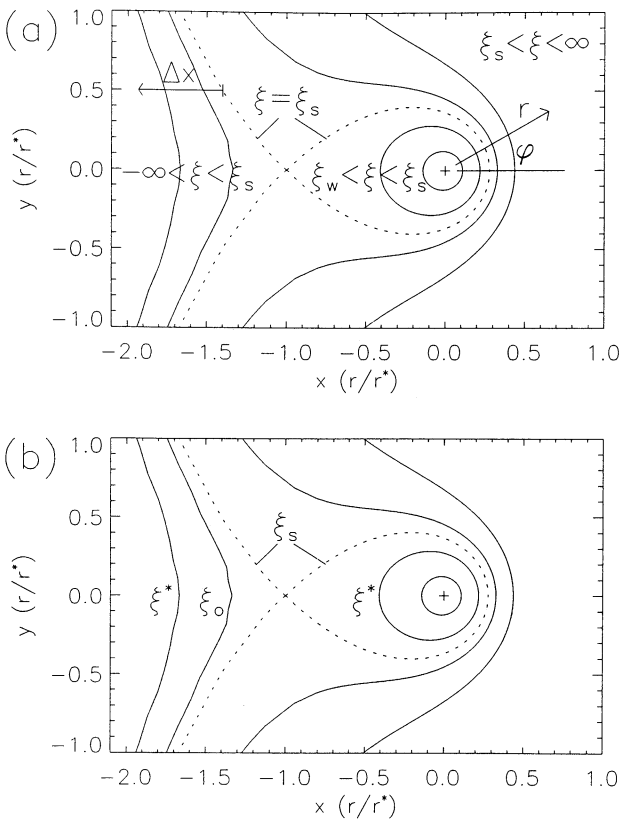

Figure 2. (a) Magnetic field lines in the x-y plane near the tether. The dotted line is the separatrix. Also shown are the values of ξ in each region delineated by the separatrix. (b) Magnetic field lines in the x-y plane near the separatrix, as discussed in Appendix A.

2.1. Generator Mode

The potential and current distributions are schematically presented in Figure 3 for a tether system operating in the generator and thruster modes. First, let us examine the current and potential distributions for a tether operating in the generator mode (Figure 3a). The closed region is proportional to the current in the wire for a chosen point along the tether, z, and expands through the segment AB. On the other hand, the potential drop between the wire and the plasma is a diminishing function on the same segment. Therefore both the strength and spatial extent of the electric field around the tether decreases along this segment. At point B, the potential difference is zero. Therefore there exists some point D along the wire where the region of strong electric field shrinks sufficiently to be contained within the separatrix. We will assume that the particle motion in the region of strong electric field (potential energy large compared to the thermal energy) is unaffected by the magnetic field. Outside of this region the particle motion is governed only by the magnetic force, resulting from the external and current-induced magnetic fields. As a result, along the segment DB the number of particles collected by the wire can not exceed the number of particles that are able to reach the region of strong electric field inside the separatrix due to their thermal motion starting from the unclosed magnetic surfaces outside the separatrix.

To calculate the electric field around the wire, the problem should be treated in a self-consistent way. However, this is beyond the scope of this study. We will assume that the potential distribution around the tether is not changed significantly due to the current-induced magnetic field and also that the OML model is still valid. Under these assumptions the region of strong electric field can be taken from the numerical calculations presented by *Laframboise and Rubinstein* [1976]. In their Figure 2 the potential distribution is presented for various ratios of electron and ion temperatures. The electric potential decreases with distance away from the wire, down to the level of the electron temperature. This distance is largest when the ions are cold. Beyond this distance, however, the potential decreases faster for cold ions than for ions with nonzero temperature. For cold ions the potential eventually becomes zero, defining the extent of the plasma sheath. The

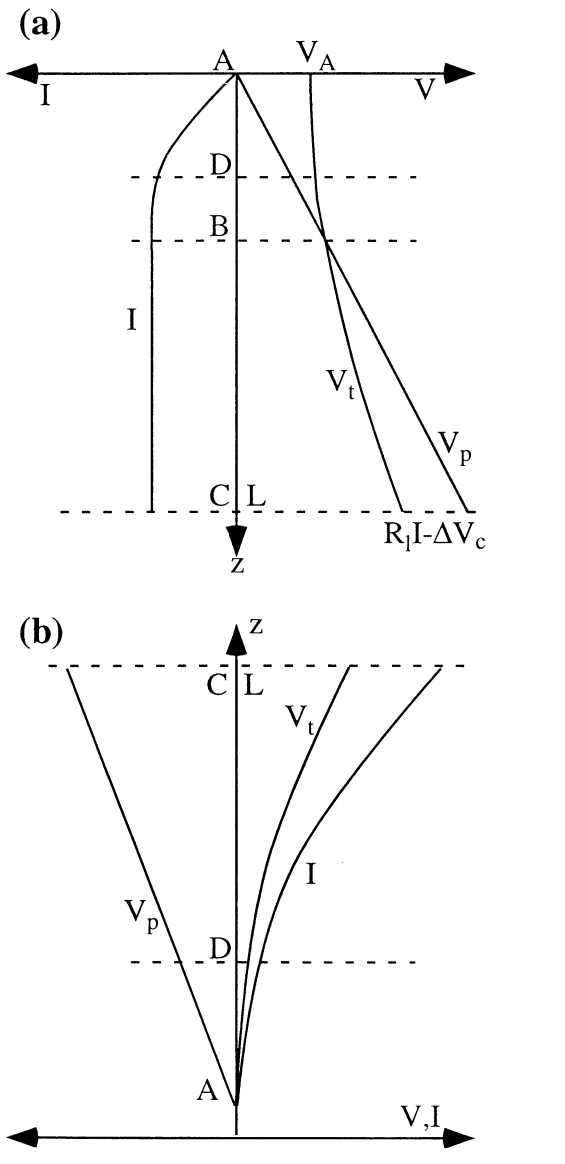

Figure 3. Schematic of the potential and current distributions along the tether for (a) generator and (b) thruster modes. Point A corresponds to the anode tether end; at point D the plasma sheath and separatrix perimeters are equal; V_t and V_p are the tether and plasma potentials in the tether reference frame. In Figure 3a, ΔV_C is the cathode potential drop; $R_l I$ is the load voltage drop; at point B the plasma and tether potentials are equal.

radius of the plasma sheath is larger than the region where the potential drops well below the electron temperature. In spite of this we will assume that the sheath radius describes the region of strong electric field. This permits us safely assume that outside the plasma sheath, the particle motion is not affected by the electric field. The effect of the current-induced magnetic field on current collection is therefore underestimated in the following calculations.

Let us put this into the context of Figure 3a. The assumption of having either strong electric fields or strong magnetic fields is applied as a function of plasma sheath and the magnetic separatrix positions in the x-y plane, but the relationship of these two boundaries to each other changes along the tether length. On segment AD, the plasma sheath is larger than the separatrix and current collection can be described by OML theory. On the segment BC, the potential repels the electrons and (because we are neglecting the ion current) there is no current collection. Along the segment DB, the plasma sheath is inside of the separatrix, and we assume that the OML-derived current collection is reduced according to the location of these two curves.

The plasma sheath radius can be found with the help of the expression presented by *Szuszczewicz and Takacs* [1979], which fits the numerical calculations of *Laframboise* [1966],

$$R_{sh}(z)=\lambda_D\left[2.50-1.54\exp\left(\frac{-0.32r_w}{\lambda_D}\right)\right]\sqrt{\frac{e\Delta V}{kT}}+r_w\,, \qquad (3)$$

where λ_D and T are the electron Debye length and temperature, ΔV is the tether potential with respect to plasma, and r_w is the wire radius.

So, we will assume that along both segments, AD and DB, the current can still be calculated according to the OML model. The difference is that on the DB segment the thermal flow reaching the edge of the plasma sheath is reduced compared to the thermal flow at infinity by some coefficient $\varepsilon(z)$. Assuming the model of the plasma sheath is a cylinder, with its radius defined by equation (3), and the closed magnetic lines are the curves presented by equation (2), we will consider that the plasma sheath and the magnetic field line coincide if their perimeters are equal. Then the point D on the wire is determined by the condition

$$S_s(z)=2\pi R_{Sh}(z) \qquad (4)$$

More details of the model are discussed by *Khazanov et al.* [2000]; the thermal flux reduction, $\varepsilon(z)$, is calculated in Appendix A.

The governing equations for the current and the potential drop along the bare tether [*Sanmartin et al.,* 1993] can easily be adapted for the described model. In the tether's reference frame of rest the electric field is $\mathbf{E}=\mathbf{u}\times\mathbf{B}_o/c$ where $\mathbf{u}$ is the tether orbital velocity. The undisturbed (motion induced) potential, V_p, in the plasma in the direction parallel to the tether is proportional to the projection of this electric field $\mathbf{E}$ along the tether direction, E_m, and thus $dV_p \sim E_m dz$. The potential resulting from IR drop inside the wire, V_t, changes in accordance with Ohm's law (like the current schematically shown in Figure 3a). Then for $\Delta V=V_t-V_p$ we have

$$\frac{d\Delta V}{dz}=\frac{I}{\pi\sigma r_w^2}-E_m\,, \qquad (5)$$

where σ is the wire conductivity. The equation for the OML current along the tether is then

$$\frac{dI}{dz}=2en_e r_w\varepsilon(z)\sqrt{\frac{2e\Delta V}{m_e}}\,, \qquad (6)$$

where n_e is the unperturbed electron density. Here, $\varepsilon(z)$ is unity for the AD segment, it is determined by formula (A7) for the segment DB, and it is equal to zero for the BC segment. For the sake of simplicity the small plasma impedance and the ion current for the segment BC are neglected. The circuit equation for the tether can then be written as

$$E_m L=\Delta V_A+\frac{1}{\pi\sigma r_w^2}\left[\int_0^{L_B} I(z)dz+(L-L_B)I_B\right]-\Delta V_C\,, \qquad (7)$$

where ΔV_A and ΔV_C are the local biases at points A and C for the anode and cathode, respectively. It is assumed that ΔV_C is known. L and L_B are the total tether length and the length of the segment AB. Equations (5) and (6) with the boundary conditions $I(z=z_A)=0$, $\Delta V(z=L)=\Delta V_C$, condition (4), the condition $\Delta V(z=z_B)=0$, and the expression (A7) constitute the complete mathematical description of the model for the tether system operating in the generator mode.

2.2. Thruster (Motor) Mode

To reformulate the model for a tether operating in the thruster mode, the needed changes are evident from the current and potential distributions along the tether (Figure 3b). The difference compared to the previous case is that at the point A, not only is the current zero but also the potential bias is small. Now both the size of the plasma sheath and the region of closed magnetic surfaces are growing functions along the tether. It can be found from equation (4) that if the tether is long enough, there will always exist a point D where the plasma sheath perimeter and the perimeter of the separatrix are equal (like in the generator mode). This is valid for any positive potential at point A and any set of system parameters. Farther from point A, the plasma sheath is inside the separatrix. Evidently, the plasma sheath can not be too far inside the boundary of closed magnetic surfaces. This will restrict the current growth along the tether but the potential will still grow. Therefore the plasma sheath will expand and move closer to the magnetic separatrix. In spite of this, the shielding effect increases, and the tether current is reduced along the tether. This is demonstrated by numerical calculations for this mode presented below.

The equations describing the thruster mode for fully and partially bare tethers are presented by *Sanmartin et al.* [1993]. For a bare tether with a positive bias, equation (6) is the same, and in equation (5) the sign of the term E_m should be changed. More details can be found in the cited paper.

3. Code Description

The mathematical problem formulated in the previous section for the generator mode is a two-point boundary value problem. Following *Sanmartin et al.* [1993], we will introduce dimensionless variables for the coordinate along the z axis, the current, and the potential as

$$l=\frac{z}{L^*};\quad L^*=\frac{3}{4e}\left[\frac{m_e E_m}{6}\left(\frac{\pi\sigma r_w}{n_e}\right)^2\right]^{\frac{1}{3}};$$

$$i=\frac{I}{\pi r_w^2\sigma E_m};\quad \phi=\frac{\Delta V}{E_m L^*}\ , \tag{8}$$

Equations (5) and (6) can then be written as

$$\frac{di}{dl}=\frac{3}{4}\varepsilon(l)\sqrt{\phi}\ ;\quad \frac{d\phi}{dl}=i-1\ . \tag{9}$$

With the help of the solution on the segment BC ($\varepsilon(l)=0$) and the first integral of equations (9) for the segment AD ($\varepsilon(l)=1$), the problem can be reduced to solving equations (9) for the segment DB. Boundary conditions at the endpoint D, taking into account the definition (4), can be expressed as functions of ϕ_A, ($l_D=l_D(\phi_A)$, $i_D=i_D(\phi_A)$, $\phi_D=\phi_D(\phi_A)$). For point B, $\phi_B=0$ and the current is given by the analytical solution along the BC segment as

$$i_B=\frac{l_C-l_B+\phi_C}{l_C(1+R_l/R_t)-l_B}\ , \tag{10}$$

where ϕ_C is known; R_l and R_t are the load and tether resistances, respectively. In all calculations the tether conductivity was determined by the expression $\sigma=\sigma_{Al}(1-0.03/r_w)$, with $\sigma_{Al}=3.5\times10^7\Omega^{-1}m^{-1}$ to take into account the protecting shell.

Equations (9) are solved on the segment DB using a fourth-order Runge-Kutta scheme. However, the calculation of ε requires a value for ξ (see Appendix A), which is found using a bisection method root solver technique and a Newton's method root solver scheme on equation $S(\xi)=2\pi R_{Sh}(z)$ (S is the length of the magnetic field line). The various integrations throughout the calculations are evaluated using Romberg's method. All of these numerical techniques are described by *Press et al.* [1986]. An initial guess for ϕ_A determines all the quantities at point D, which are then used to begin the Runge-Kutta calculation from D to B. The resulting current at B is compared against the value from equation (10), ϕ_A is adjusted in the appropriate direction, and the process is iterated until the two values of i_B (from the Runge-Kutta solution and from equation (10)) converge.

For the thruster mode the problem is simpler because it can be formulated as an initial value problem with a known potential and current values at point A.

The results without a current-induced magnetic field are found by setting $\varepsilon=1$ from point D to point B for the generator mode and all along the tether for the thruster mode. An iteration is still needed for these calculations because the initial guess for ϕ_A must be adjusted until the two values for i_B converge. However, the calculation is simpler because no flux reduction is applied.

Table 1. System Parameters

Parameter	Dimension	Values (or range)
L	km	3-20
r_w	mm	0.6-2.75
n_e	cm^{-3}	8.4×10^5-10^7
B_o	nT	2.5×10^4, 3.7×10^4
α	Degrees	1°-70°
R_l/R_t		0, 1, 2
$E=\lvert\mathbf{u}\times\mathbf{B}_o\rvert/c$	V/km	65, 170, 260

Table 2. Dependence of Current Reduction on the Plasma Density for the Unloaded and Loaded Regimes

n_e, cm^{-3}	I_0,[a] A	I, A	$(I_0-I)/I$, %
	Unloaded Regime [b]		
0.84×10^6	16.9	16.7	1
1.67×10^6	25.6	23.0	11
3.34×10^6	31.9	25.8	24
6.68×10^6	34.5	26.5	30
10.0×10^6	35.2	26.5	33
	Loaded Regime [c]		
1.67×10^6	22.5	21.6	4
3.34×10^6	27.3	24.7	11
6.68×10^6	30.7	26.1	18
10.0×10^6	32.2	26.4	22

[a] I_0 in this table and those below is the current calculated neglecting the current-induced magnetic field.

[b] Parameters are as follows: $r_w=1.8$ mm, $L=5$ km, $\alpha=60°$, $E_m=130$ V/km, and $R_l/R_t=0$.

[c] Parameters are as follows: $r_w=2.5$ mm, $L=5$ km, $\alpha=60°$, $E_m=130$ V/km, and $R_l/R_t=1$.

4. Results and Discussion

The main goal of the numerical calculations presented below is to outline the domain of system parameters for which the current-induced magnetic field can reduce the current collected by a tether operating in the generator and thruster modes for reasonable current magnitudes. The dependence on plasma density, angle between the tether and the external magnetic field, the tether length, and tether radius was analyzed for the domains presented in Table 1. Three configurations for the spacecraft velocity and the external magnetic field, given in Table 1, were used. Plasma densities, temperature, external magnetic field, spacecraft velocity, and tether orientation in this table where chosen taking into account the ProSEDS mission operation modes. These values span the nominal range for each of these parameters in which the ProSEDS tether will operate.

4.1. Generator Mode

In all calculations for the generator mode, unless stated otherwise in the figure caption, the point C was assumed to be at a local bias of minus 30 V (ΔV_C), the external magnetic field (B_o) was set to 3.7×10^4 nT, and the temperature was taken to be 1900 K. Below, results are presented for both a loaded ($R_l/R_t=1$) and an unloaded ($R_l/R_t=0$) tether.

The general character of changes in the current and potential distributions along the tether due to the current-induced magnetic field for this mode can be seen in Figures 4, 6, and 7. In

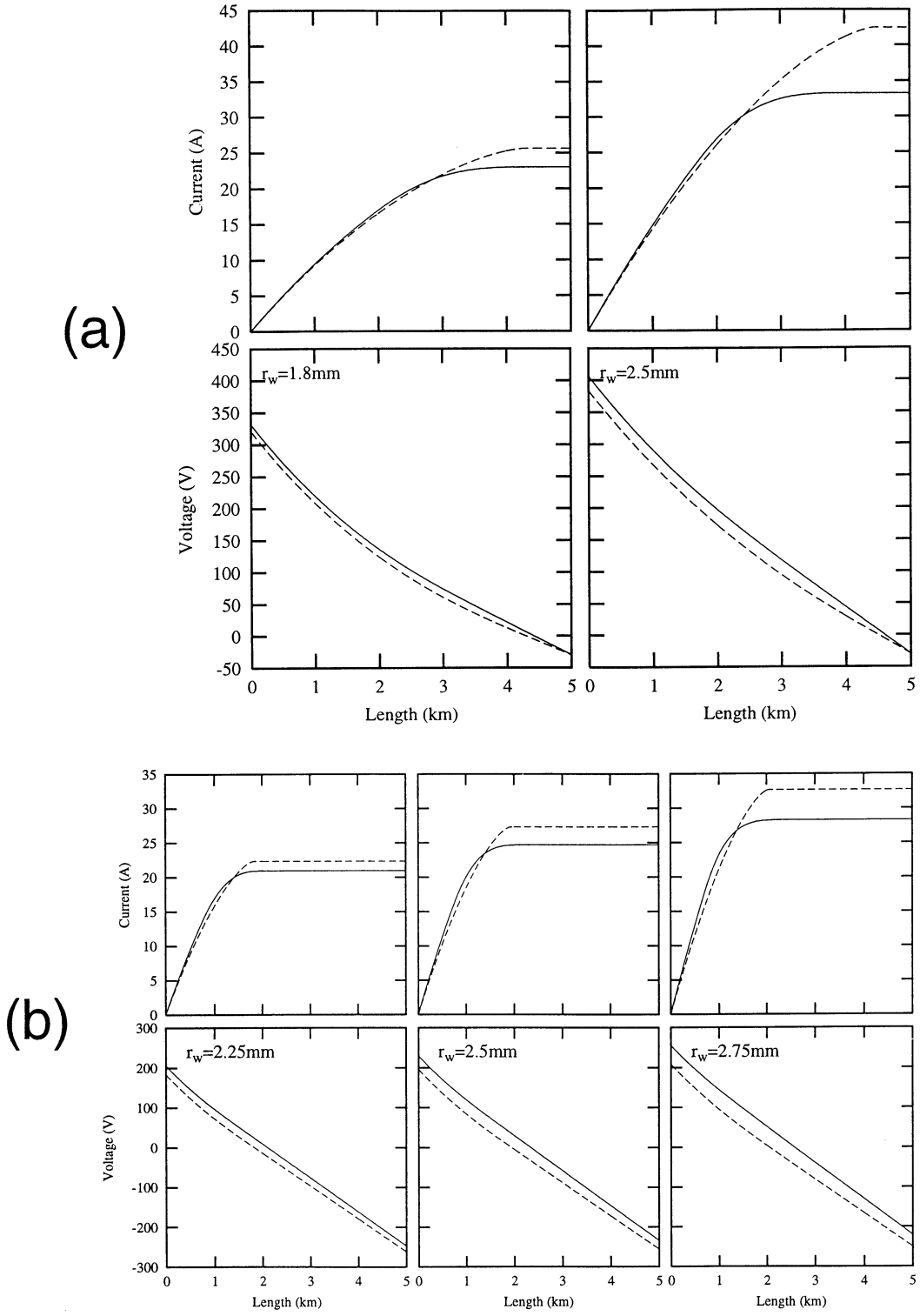

Figure 4. Generator mode. (a) Dependence of current reduction on the tether radius for the unloaded regime with n_e=1.67×10^6 cm^{-3}, α=60°, and E_m=130 V/km; in all figures the dashed line presents the calculations without the self-induced magnetic field. (b) Dependence of current reduction on the tether radius for the loaded regime, R_l/R_t=1. For n_e =3.34×10^6 cm^{-3}, α=60°, and E_m=130 V/km.

all cases (both a loaded and unloaded tether), the potential obtained from equation (5) for the endpoint A with respect to the plasma potential, ΔV, is higher when the magnetic shielding is taken into account. Because of this, the collected current is larger along the segment AD than in the cases without the current-induced magnetic field presented in the same figures by dashed lines. The total collected current in all cases is reduced because of the current-induced magnetic field. The shape of the potential distribution for an unloaded tether in some cases is essentially changed due to a larger potential drop along the part of the tether close to point A. The changes depend on the tether system parameters listed above.

4.1.1. Density dependence. It is evident from the described model that the limiting effects of the self-induced magnetic field on tether current collection should strongly depend on plasma density. For increasing density, the Debye length (and, therefore, the plasma sheath) contracts while the current increases and the separatrix length grows, therefore, extends outward. As a result, the effect of current-induced magnetic shielding reduction should be essentially greater for larger densities. This is what we see in Table 2 for the unloaded tether and for the same tether with a load resistance, $R_l/R_t=1$. For the unloaded tether (Table 2, top) the second column gives the total collected current neglecting the effects of the current-induced magnetic field, I_0. The next column gives the current subject to magnetic shielding, I. Notice that I_0 grows more rapidly with plasma density than I. As a result, the current reduction (the right column in the table) quickly grows with density. The tendency toward saturation for both currents for large plasma densities is more profoundly expressed for the case with the current-induced magnetic field.

The loaded tether (Table 2, bottom) behaves qualitatively like the unloaded tether (Table 2, top) except that the current reduction is smaller because the load restricts the magnitude of the current and, therefore, the strength of the self-induced magnetic field. As a result, the effect of current reduction for the loaded tether is reduced and is significant only for sufficiently large densities.

4.1.2. Dependence on the wire radius. The role of the wire radius is illustrated in Figures 4a and 4b for the unloaded and loaded regimes, respectively. Note that if the resistance is neglected the potential is independent, while the current is directly proportional, to the wire radius. Therefore, for two tethers of the same length and different radii the potential distribution along the tether is the same. The current and the region of closed magnetic surfaces around the tether are larger for the tether with the larger radius and, therefore, the current

Table 3. Dependence of Current Reduction on the Tether Length for the Unloaded and Loaded Regimes

L, km	I_0, A	I, A	$(I_0-I)/I$, %
	Unloaded Regime [a]		
3	15.1	14.5	4
5	25.6	23.0	11
10	35.3	31.2	13
20	37.4	35.2	6
	Loaded Regime [b]		
3	21.0	19.2	9
5	27.3	24.7	11
10	32.9	30.3	9
20	35.9	34.0	6

[a]Parameters are as follows: $r_w=1.8$ mm, $n_e=1.67\times10^6$ cm^{-3}, $\alpha=60°$, $E_m=130$ V/km, and $R_l/R_t=0$.

[b]Parameters are as follows: $r_w=2.5$ mm, $n_e=3.34\times10^6$ cm^{-3}, $\alpha=60°$, $E_m=130$ V/km, and $R_l/R_t=1$.

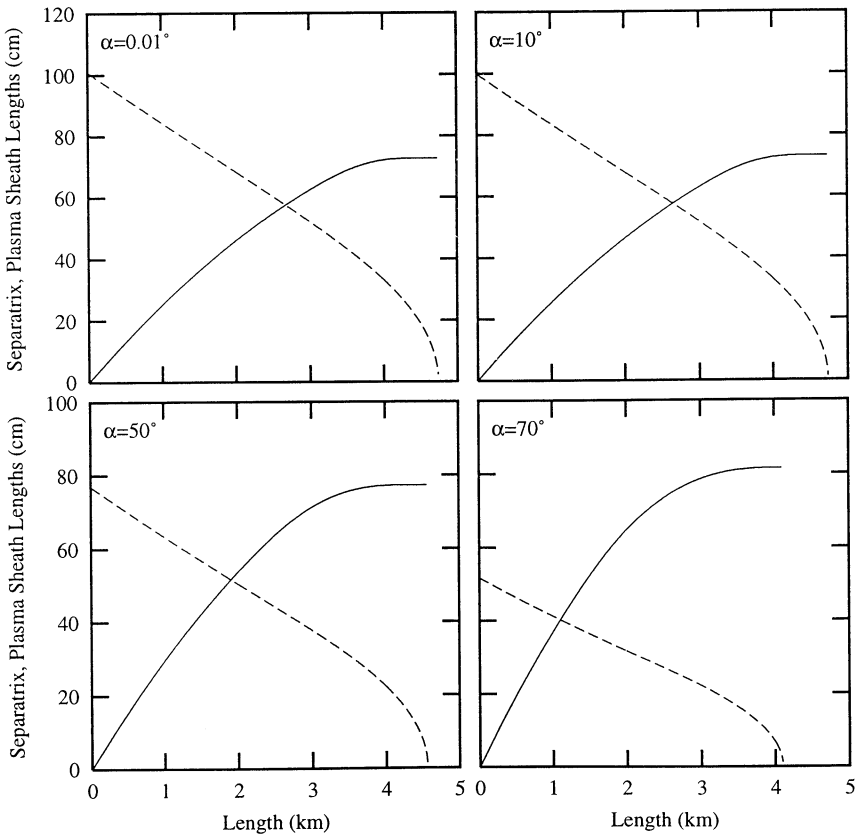

Figure 5. Generator mode. Dependence of the plasma sheath and separatrix lengths on the angle between the tether and the external magnetic field. Alpha is the complement angle, that is, the angle between this field and the plane perpendicular to the tether. The solid line belongs to the separatrix. Here $n_e=1.67\times10^6$ cm^{-3}, $r_w=1.8$ mm, $E=260$ V/km, and $R_l/R_t=0$.

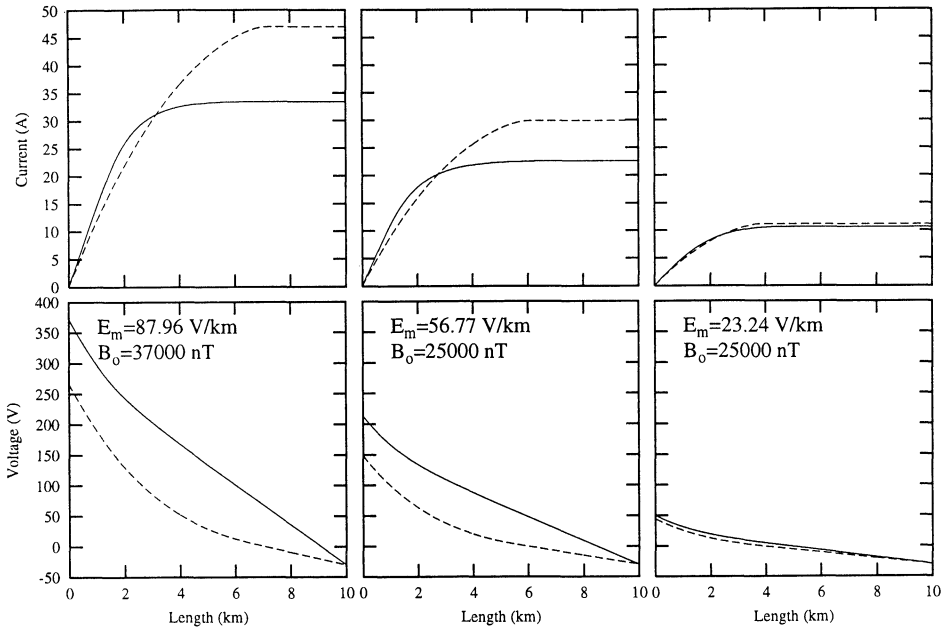

Figure 6. Generator mode. Dependence of current reduction on the external magnetic and induced electrical fields for n_e=1.67×10^6 cm^{-3} , r_w=2.5 mm, α=70°, and R_l/R_t=0.

reduction for this tether is greater. Thus Figures 4a and 4b simply reflect the fact that even if the tether resistance is taken into account, the dependence of the current on tether radius is still qualitatively the same. It can be seen from these figures that the dependence on radius is strong. When the radius increases from 1.8 mm to 2.5 mm, the reduction of current resulting from magnetic shielding, $(I_0\text{-}I)/I$, grows from 11% to 28% for the unloaded tether. The same tendency holds for the loaded tether (Figure 4b), but the magnitude of current reduction is smaller. (Note that, in this case, the plasma density was taken to be 2 times greater than for the previous case of the unloaded tether.) When the wire radius changes from 2.25 mm up to 2.75 mm, the current reduction grows from 4% to 16%, respectively.

4.1.3. Dependence on the tether length. Table 3 presents the dependence of current reduction on the tether length for the unloaded and loaded cases. For both cases, current reduction is less for short (3 km) and long (20 km) tethers than for tethers of intermediate lengths. The maximum of current reduction is displaced toward shorter tether lengths for the loaded case. For both the loaded and unloaded regimes the tendency for current saturation to occur for long tethers plainly results from the finite tether conductivity. The potential drop between the ends of a longer tether is larger, and, therefore, larger currents can be expected. But the bulk of the current is collected near the end of the tether where the potential of the tether with respect to the plasma is high, as can be seen from Figures 4, 6, and 7. As a result, the ohmic losses grow quickly with tether length, thereby lowering the maximum attainable current, which leads to current saturation.

4.1.4. Dependence on the angle between the tether and the external magnetic field. In principle, the role of the angle between the tether and the external magnetic field in the reduction of tether current can be understood from the model. Diminishing angles between the tether and the external magnetic field reduce the potential between the tether and plasma. As a result, the radius of the plasma sheath is also reduced. The dependence of the separatrix length on this angle is more complicated. For a given tether current, the region of closed magnetic surfaces should expand as the component of the external magnetic field perpendicular to the tether decreases. Simultaneously, however, the reduction of the component of the external magnetic field perpendicular to the tether reduces the current in the tether, thereby weakening the induced magnetic field. Neglecting tether resistance, we find that the length of the separatrix grows as $1/\cos^{1/2}\alpha$, notwithstanding the decrease in tether current. How this simple picture changes when the wire resistance and current reduction are included in the consideration is not evident. As can be seen from Figure 5, the separatrix is still growing with angle as the

Table 4. Dependence of Current Reduction on the Angle Between the External Magnetic Field and the Plane Perpendicular to the Tether for the Unloaded and Loaded Regimes

α, deg.	I_0, A	I, A	$(I_0\text{-}I)/I$, %
	Unloaded Regime [a]		
10°	44.5	41.7	7
50°	31.8	28.8	10
60°	25.6	23.0	11
70°	18.1	16.2	12
	Loaded Regime [b]		
30°	55.9	51.9	8
60°	32.9	30.3	9
70°	22.6	21.0	8

[a]Parameters are as follows: r_w=1.8 mm, L=5 km, n_e=1.67×10^6 cm^{-3}, E_m=130 V/km, and R_l/R_t=0.

[b]Parameters are as follows: r_w=2.5 mm, L=10 km, n_e=3.34×10^6 cm^{-3}, E_m=130 V/km, and R_l/R_t=1.

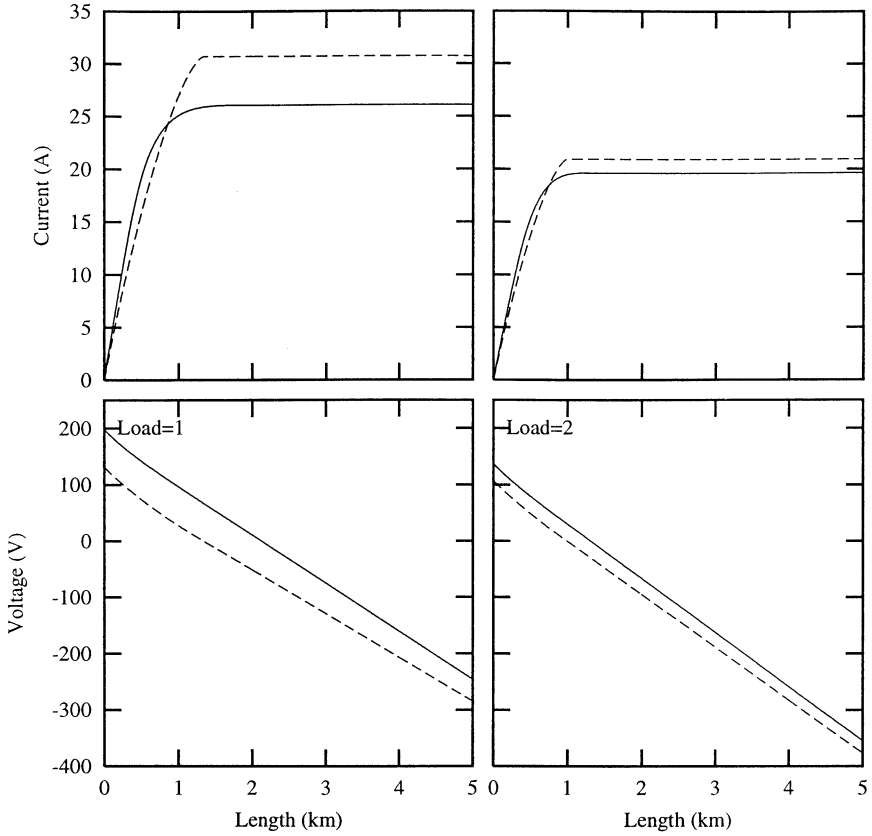

Figure 7. Generator mode. Dependence of current reduction on the load. Here n_e=6.68×10^6 cm^{-3}, r_w=2.5 mm, α= 60°, and E_m=130 V/km; loads 1 and 2 correspond to R_l/R_t=1,2.

plasma sheath contracts. However, the growth of the separatrix length is essentially smaller than the reduction of the plasma sheath length. Therefore the main factor in the dependence of the current reduction on the angle between the tether and the external magnetic field is the reduced extent of the plasma sheath for a practically unchanged separatrix length. The results are presented in Table 4. For the unloaded tether (Table 4, top), the current reduction is a slowly growing function of the angle α, in agreement with what was said above. This dependence practically vanishes for the loaded case (Table 4, bottom). In the latter case the reduction in current is much less than 10% if smaller densities and wire radii are concidered.

4.1.5. Dependence on the external magnetic field and induced electric field *E*. This dependence is illustrated in Figure 6. The left and middle columns differ by the magnitude of the external magnetic field, 3.7×10^4 nT and 2.5×10^4 nT respectively, with the proportional difference in E and E_m. (Note that the angle α for all cases in this figure is the same.) The current calculated with and without the current-induced magnetic shielding changes almost exactly in the same proportion as the external magnetic field. The current reduction for the larger field is greater, 41%, than for the smaller field, 32%. The values in the right column correspond to a much smaller E and E_m and, therefore, current- and the magnetic shielding effect is only about 5%. Such a small E corresponds to an angle between the spacecraft velocity and external magnetic field ≈25°. In contrast, this angle for the first and second columns is ≈77°. Such changes are expected as a tether system in the ionosphere moves about its orbit, particularly those with high inclinations.

4.1.6. Dependence on the load resistance. As was described above, the load in all cases diminishes the tether current and, therefore, the effectiveness of the self-induced magnetic shielding. Correspondingly, the tether current reduction is also less for a loaded tether and the effect becomes significant only for larger plasma densities and wire radii (which increase the current and offset the effect of the load). The dependence on load is presented in Figure 7. The current reduction diminishes from 18% to 6% when the load increases from being equal to, to being 2 times the tether resistance.

4.2. Thruster (Motor) Mode

For the thruster mode the local bias (ΔV_A) at the point A in Figure 3b was taken to be zero, the external magnetic field (B_o) was assumed to be 2.5×10^4 nT, and the motional emf (E) is 65 V/km, except for the cases where other values are explicitly stated in the figure captions. In all figures the short vertical line marks the tether length where current reduction from magnetic shielding reaches 10%.

As stated above, if the tether is sufficiently long, and any positive potential is imposed at the endpoint A, magnetic shielding will occur starting from some point D along the tether. The length of the segment AD and the required voltage depend on the system parameters. For this mode, both the tether current and potential are lowered by the effect of the current-induced magnetic field. The main distinction between the

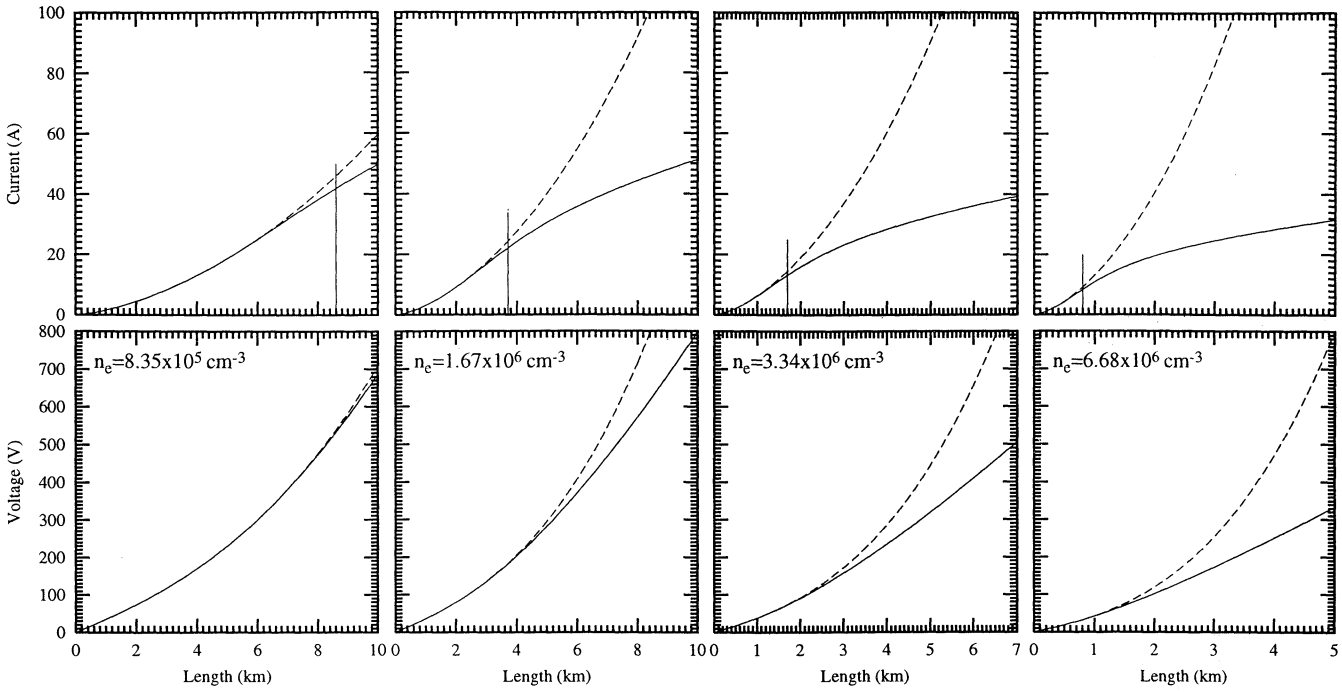

Figure 8. Thruster mode. Dependence of current reduction on the plasma density for r_w=2.5 mm, α=60°, and E_m=34 V/km.

thruster and generator modes is that in the thruster mode there is no longer a point on the tether where the potential changes sign and, therefore, the potential is everywhere positive and an electron current is collected over the entire length of the tether.

Because the solution of the equations is completely determined by the boundary conditions at point A, the results describe, not only the fully bare tether, but also the partly insulated one. The current for the partially insulated tether is simply the current from a figure presenting the results for the bare tether taken at the point corresponding to the length of the bare segment. This approach is also valid for determining the potential drop on the bare part of the partially insulated tether. The total potential drop across the insulated part of the tether can be calculated from a simple application of Ohm's law using the fixed value of current for this segment.

The dependence of magnetic shielding on system parameters for a tether operating in the thruster mode is usually similar to the dependence discussed above for the generator mode. The density dependence is presented in Figure 8. Compare to

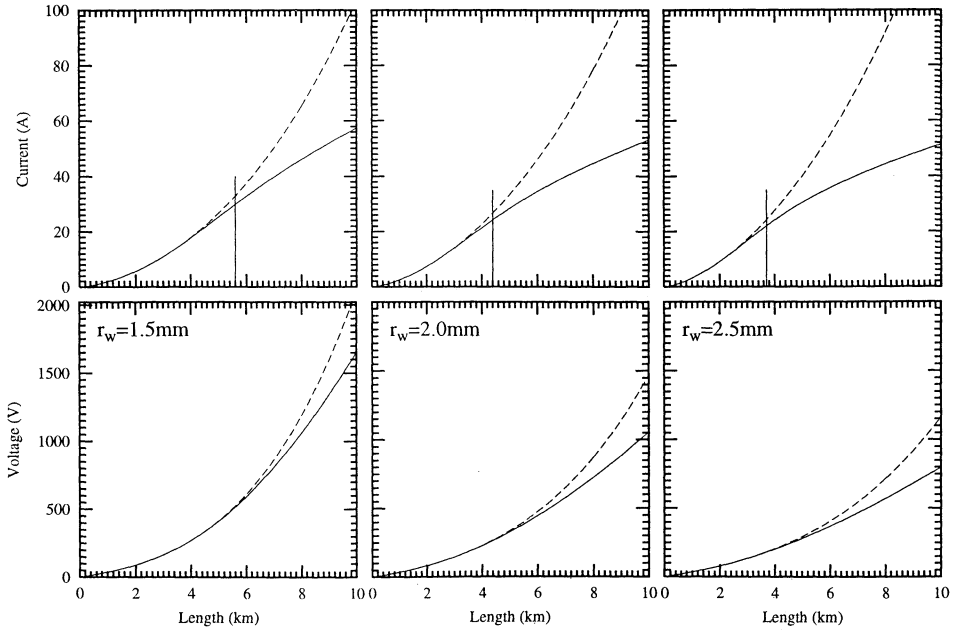

Figure 9. Thruster mode. Dependence of current reduction on the tether radius for n_e=6.68×10^6 cm^{-3}, α=60°, and E_m=34 V/km.

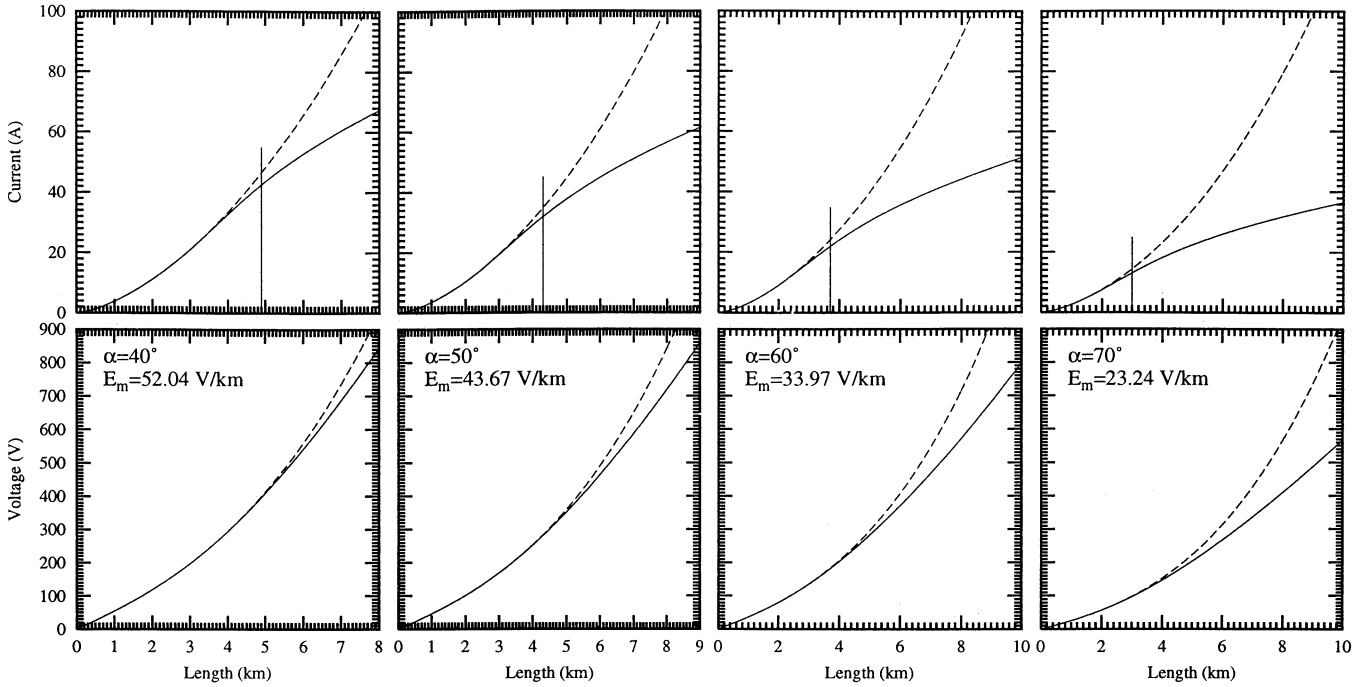

Figure 10. Thruster mode. Dependence of current reduction on the angle between the tether and the external magnetic field. Alpha is the angle between this field and the plane perpendicular to the tether. Here n_e=1.67×10^6 cm^{-3} and r_w=2.5 mm.

the case of the generator mode, a density increase leads to significantly greater shielding and therefore larger current reduction. As can be seen from the figure, when the density increases, the 10% mark shifts to a shorter tether length. Simultaneously, as a result of the density increase, magnetic shielding becomes meaningful at a much lower values of tether current and potential.

Similar changes are seen when the wire radius is increased (Figure 9). The shielding effect can be significant for a smaller radius in the thruster mode than in the generator mode. The same tendency holds when the angle between the tether and the external magnetic field diminishes, as can be seen in Figure 10. The effect is stronger for smaller angles for the same reasons given for the angular dependence of the generator mode.

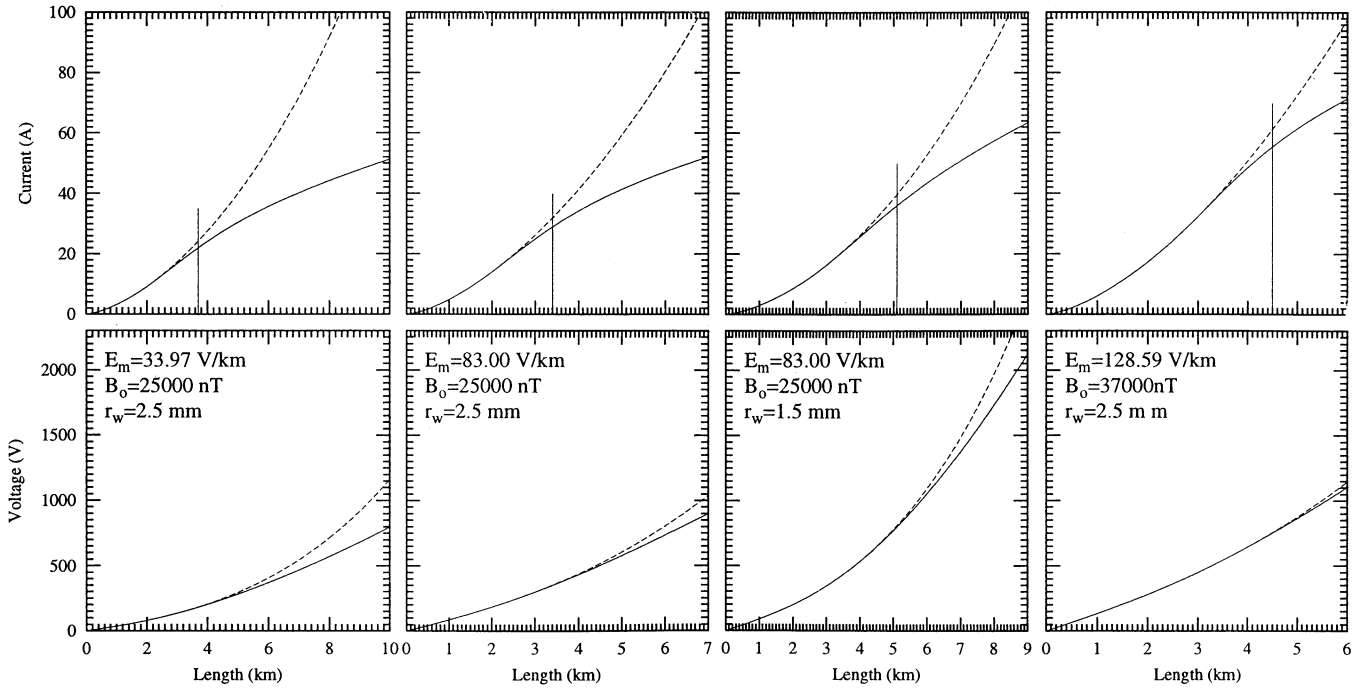

Figure 11. Thruster mode. Dependence of current reduction on the external magnetic and induced electrical fields for n_e=1.67×10^6 cm^{-3} and α=60°.

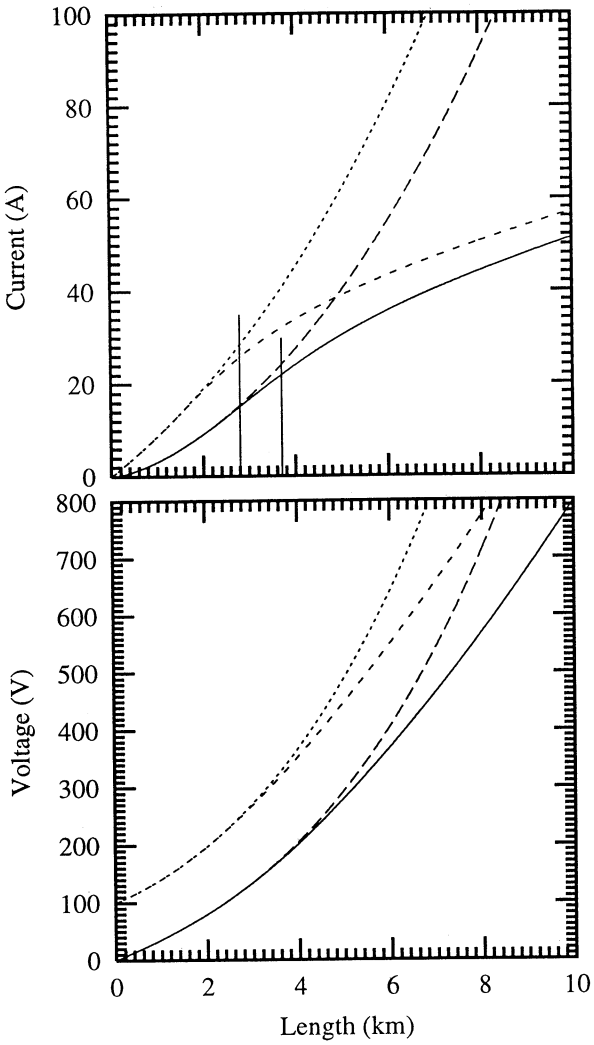

Figure 12. Thruster mode. Dependence of current reduction on the potential at the endpoint A, showing results with V_A=100 V (short-dashed and dotted lines) and V_A=0 (long-dashed and solid lines). The dotted and long-dashed lines are without self-induced effects, while the other two include them. For these results, n_e=1.67×10^6 cm^{-3}, α=60°, r_w=2.5 mm, and E_m=34 V/km.

A dependence that is completely different between the thruster and generator modes is the current reduction dependence on the external magnetic and induced electric fields. As can be seen in the first and second columns from the left in Figure 11, the growth of E and E_m, as a result of increasing the angle between the external magnetic field (fixed magnitude and α) and the orbital velocity vector, not only moves the 10% mark farther from the endpoint, but also increases the current for which such reduction is reached. The third column from the left differs from the second only by the wire radius. When the magnitude of the external magnetic field (α is fixed) and E are both enlarged, the 10% mark moves to significantly larger currents and tether lengths, as can be seen from the rightmost column.

Up to now, the discussion of the thruster mode has concerned only the case where the potential at the endpoint of the tether, A, is zero. The change that occurs when the potential at point A has a non-zero value is illustrated in Figure 12. When V_A=100 V, the 10% mark moves closer to the endpoint A, and the current simultaneously grows. This result is evident from the model because the current and the separatrix are growing more quickly along the tether due to the increased starting potential.

For some combinations of system parameters magnetic shielding can result in a very strong reduction of the tether current. Such an example is presented in Figure 13 for the thruster mode. In this case the 10% reduction point is reached at a length of 0.65 km for a tether current of 4.3 A, and increases to over 40% at twice this distance up the tether.

As can be seen from these results for the thruster mode, current-induced magnetic shielding of the tether, and a corresponding reduction of the collected current, can be expected for relatively small currents and becomes important for relatively short tethers.

5. Summary

The goals of the parametric study, presented in the previous section, are to determine (1) the parameters of the tether-ambient plasma system that govern the self-induced magnetic shielding, and (2) the parametric domain for which the reduc-

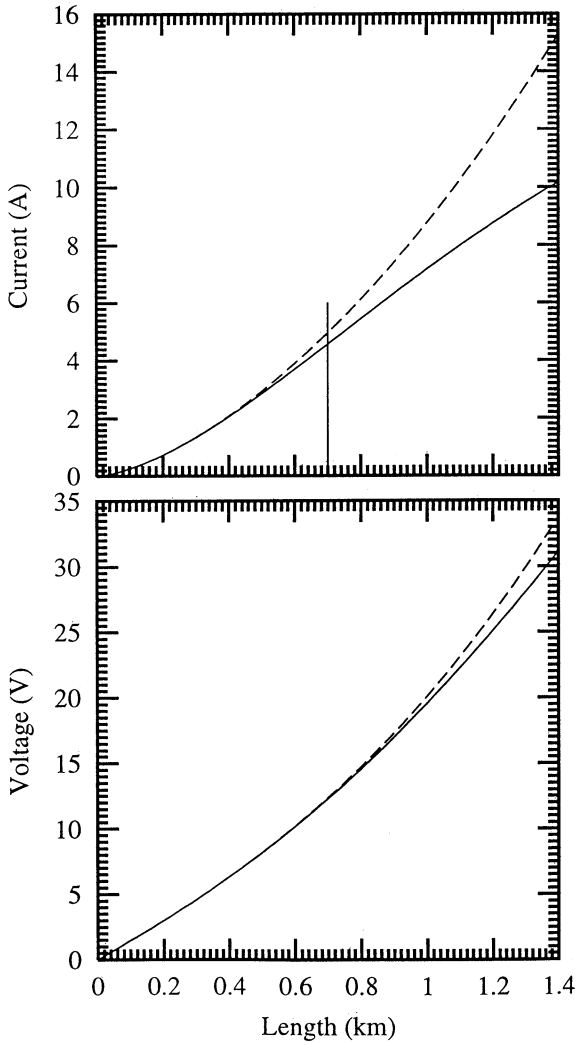

Figure 13. Thruster mode. Here n_e=6.68×10^6 cm^{-3}, α=70°, r_w=2.5 mm, and E_m=34 V/km.

tion of the collected current, $(I_0-I)/I$, as a result of magnetic shielding, has a significant impact on the performance of a tether operating in either the generator or thruster (motor) modes. We define a "significant" impact to be 10% or greater. The parametric dependencies of current-induced magnetic shielding on the collection of current for bare tethers with radii up to 2.75 mm and lengths up to 20 km are as follows:

1. Current-induced magnetic shielding essentially depends on the magnitude of the tether current and, therefore, responds to any parametric change that in turn affects current levels in the tether.
2. In general, the effect of current reduction becomes more significant for a tether operating in the thruster mode than in the generator mode, at least for values of E_m that are not too large.
3. As a rule, current reduction from magnetic shielding can be significant for a tether operating in the generator mode if the current is greater than 15 A.
4. The current reduction for a tether operating in the generator mode strongly depends on the load resistance. For the parametric range studied, the reduction of current was not significant if the load resistance was more than 2 times the resistance of the tether.
5. The degree of magnetic shielding essentially depends on the plasma density. The shielding is obviously negligible for a tether operating in the generator mode under conditions of the highly rarefied nightside ionosphere. However, for the more sensitive thruster mode, the effect is significant for the lower plasma densities and could be significant under these conditions.
6. The current reduction for both operational modes strongly depends on the tether radius and conductivity and quickly grows as these parameters increase. The smallest radius for which magnetic shielding is still significant in the generator mode was found to be around 1.8mm for a dayside ionospheric density of 1.67×10^6 cm^{-3}. The minimum radius is even smaller for a tether operating in the thruster mode in plasma of the same density.
7. For the generator mode the current reduction is greater for smaller angles between the tether and external magnetic field $(90°-\alpha)$. The angular dependence is much stronger for the thruster mode than for the generator mode, and can significantly reduce the length of the segment required for the shielding effect to reach the 10% level.
8. The dependence of the shielding effect on the tether length is weak for the generator mode and the current reduction diminishes for long (20 km) and short (3 km) tethers. It is less evident in the cases with load. For the thruster mode the shielding effect has a strong dependence and grows quickly with the length.
9. The shielding effect is enhanced for a tether operating in the thruster (motor) mode by placing a positive potential at the collecting end of the tether.
10. The dependence of the magnetic-field-induced current reduction on the external geomagnetic field and its orientation with respect to the spacecraft velocity vector are different for the generator and thruster modes. Current reduction is greater for the generator mode under the conditions of larger external magnetic field and induced electric field E. The opposite is true for the thruster mode.

In all cases (except the loaded generator mode) we have avoided the presentation of results when all the parameters are acting in favor of self-induced magnetic shielding. Our results, therefore, do not maximize the magnetic shielding effect. In the case of the generator mode, the domain of such parameters is not too large and can lead to a large increase in current reduction when large densities occur in conjunction with a large tether radius and a small angle between the external magnetic field and the tether. For a tether operating in the thruster mode this domain is larger. An example of such strong shielding for the thruster mode is shown in Figure 13. In this case, the 10% mark for current reduction is reached for the current 4.5 A at 0.7 km along the tether and the reduction quickly increases with length beyond this point.

As stated in section 1, two changes are introduced in the present model of current-induced magnetic shielding of a bare tether compared to *Khazanov et al.* [2000]: (1) finite tether conductivity is included, and (2) a more accurate description is made of the electron flow through the separatrix. In the earlier model, it was assumed that if the plasma sheath radius at a given point on the tether was less than the extent of the separatrix by more than the Larmor radius, electrons could not reach the tether from infinity and the incremental current was set to zero. Instead of equation (4), the expression $0.3r-r_{Le}=R_{Sh}$ was used in that study. The present model, in the limit as tether conductivity goes to infinity, yields results that are close to those presented in *Khazanov et al.* [2000]. For example, the ratio of the tether current calculated with and without current-induced magnetic field shielding effect, presented by *Khazanov et al.* [2000] in their Figure 3, is 63%. The present model, for the same system parameters, gives a ratio of 57%. The domain of parameters where such agreement holds true has not yet been fully established.

As was stated above, there are two main purposes of the presented calculations. The first is to demonstrate that the current-induced magnetic field can be an essential factor in determining tether current collection. The second is to analyze the dependence of the self-induced magnetic shielding effect on the tether system and ambient plasma parameters while eliminating the idealization of infinite conductivity used by *Khazanov et al.* [2000].

Owing to the current in the wire, the magnetic field around the tether is split into two domains. The region near the tether is disconnected from infinity (if the end effects are neglected), and the particle transport to the tether in this region is possible only across the magnetic field lines. It was assumed that the electric field around the tether could also be divided in to 2 regions: an inside region of strong electric field near the tether where electron motion is unaffected by the magnetic forces, and an outside region where electron motion is governed by the external magnetic field, and the electric field is weak and can be neglected.

As in the theory of the bare tether of *Sanmartin et al.* [1993], we assume that the potential distribution near the tether is such that the conditions of OML theory are satisfied in spite of the more complex magnetic field geometry in this case. The particle velocity distribution is assumed to be three-dimensional. This assumption is based on the results of *Laframboise and Rubinstein* [1976], where they demonstrated that even in the adiabatic limit a three-dimensional distribution leads to the "correct density expression for noncollection orbits" [*Laframboise and Rubinstein*, 1976, p. 1904]. A more complicated geometry of the magnetic field in our case favors this conclusion.

The region of strong electric field was calculated with the help of the expression from *Szuszczewicz and Takacs* [1979],

which fits the numerical results of *Laframboise and Rubinstein* [1976] for cold ions; that is, the region of strong electric field was identified with the region of the plasma sheath. As can be seen from the numerical results of *Laframboise and Rubinstein* [1976], this region is much larger than the region where the potential decreases below the electron temperature (when the ion temperature is taken into account). Therefore outside this enlarged region, that is, outside the plasma sheath, the particle motion is not affected by electric field. Based on this, it was assumed that when the edge of the plasma sheath is inside the separatrix dividing closed and unclosed magnetic regions, the current is orbit limited, but the random flux at the edge of the plasma sheath is reduced to the thermal flux across the magnetic field lines.

As a result of these assumptions it can be supposed that the role of the current-induced magnetic field on current collection is underestimated in the presented calculations. Likewise, the effect is underestimated if the potential around the tether drops more abruptly than is supposed by OML theory. A self-consistent calculation of the problem is needed to justify these conclusions and more accurately calculate the reduction of current collected by the tether. In addition, other questions arise, such as, What is the role of plasma turbulence; that is, does the shear of the combined external and current-induced magnetic fields change the plasma stability? What is the possible role of the closed magnetic surfaces with regard to ionization? Additional study is also needed to address such issues that are beyond the scope of the present model.

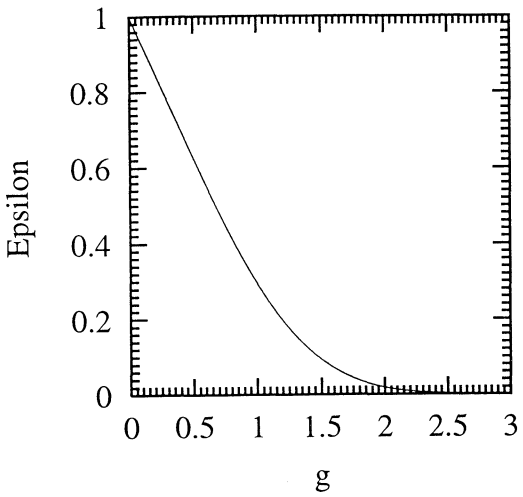

Figure 14. The reduction coefficient $\varepsilon(g)$.

Appendix A

To determine the current reduction, $\varepsilon(z)$, on the DB segment in equations (6) and (9), the fraction of the thermal flow from outside the separatrix reaching the closed magnetic field line ξ corresponding to the edge of the plasma sheath inside the separatrix, defined by equation (3), should be calculated. Two conservation laws restrict the particle motion in the magnetic field presented by equations (1) and (2) and shown in Figure 2, for the z component of the particle generalized momentum and for the particle energy. Assuming the collected particles are electrons, this yields

$$P_z=m\dot{z}+\frac{e}{c}A_z=m\left(v_z+\Omega\xi\right)=\text{const}, \tag{A1}$$

where $\Omega=|e|B_o/mc$, and

$$E=\frac{m}{2}\left(\dot{r}^2+r^2\dot{\varphi}^2+\dot{z}^2\right)=\text{const}. \tag{A2}$$

Then the particles starting at infinity from the field lines with ξ_o are able reach the point (r,φ) on the field line ξ, closer to the wire, if ξ_o satisfies the inequalities

$$\xi_-\le\xi_o\le\xi_+ \tag{A3}$$

where

$$\xi_\mp=\xi-(1/\Omega)\left(v_{oz}\pm\sqrt{2E/m}\right).$$

The inequalities in equation (A3) follow from equations (A1) and (A2) under this condition on the velocity component perpendicular to the wire for a particle on the field line ξ: $v_{\perp\xi}\ge 0$, and also taking into account that the energy at infinity is positive. These inequalities should be supplemented by the condition that the electrons are starting from ξ_o outside the separatrix, ξ_s. The region $\Delta x(v_o,v_{oz})$ at infinity ($y_o\to-\infty$) from which the particle with given v_o and v_{oz} is able to reach the line ξ is simply related to the restricting field lines (A3) [see *Khazanov et al.*, 2000]:

$$\Delta x_o=\frac{\xi_+-\xi_-}{\cos\alpha}. \tag{A4}$$

We will assume that the particle velocity distribution is Maxwellian and the plasma is collisionless; that is,

$$f(v)=n_e\frac{m}{(2\pi T)^{3/2}}\exp\left(-\frac{mv^2}{2T}\right). \tag{A5}$$

Also, it is assumed that far from the wire ($y_o\to-\infty$) electrons have orbits that are helical and move along the external magnetic field lines. Then according to the paper of *Rubinstein and Laframboise* [1978], the flux per unit length along the z axis due to the electrons collected from the interval Δx_o is given by the expression

$$I=4\pi e\int_0^{\frac{\pi}{2}}\sin\theta d\theta\int\Delta x_o(v,\theta)f(v)v\cos\theta\cos\alpha v^2dv. \tag{A6}$$

Here a spherical coordinate system with polar axes along the magnetic field line is introduced for the velocity space description at infinity. The term $v\cos\theta\cos\alpha$ is the component of electron velocity in the plane transverse to the tether averaged over a gyroperiod. The domain of integration for θ selects electrons flowing toward the tether. Analyses of inequalities (A3) to obtain the domain Δx_o from expression (A4) should take into account that for electrons moving from the left-hand side (Figure 2a) ξ grows, reaches a maximum on the separatrix, and then diminishes.

The inequalities (A3) split the phase space of integration in equation (A6) into three domains depending on the ratio between ξ_o (starting field line), ξ^* (a field line inside the separatrix), and ξ_s (the field line of the separatrix). For example, let the particle start from the line $\xi^*<\xi_o<\xi_s$ outside the separatrix, and it should reach the line ξ^* inside the separatrix (note that ξ is a two-valued function of the coordinates, see

Figure 2b). Then from the condition that inequalities (A3) should be satisfied on every line crossed by the particle trajectory, it follows that ξ_o should belong to the range

$$-(v_o+v_{oz})/\Omega-\xi_s<\xi_o<\xi_s,(v_o-v_{oz})/\Omega+\xi^*$$

where $v_{oz}=v\cos\theta\sin\alpha$. Now the regions of integration on ξ_o, v_o, and θ can be found and the flux, given by equation (A6) for this domain, can be calculated. The flux, summed up over all domains permitted by inequalities (A3) and divided by the total flux on the separatrix (flux from equation (A6) calculated for $\xi=\xi_s$), leads to the expression for flux reduction inside the separatrix

$$\varepsilon(z)=\frac{2g}{3\sqrt{\pi}}e^{-g^2}+\mathrm{erfc}g\ , \qquad \text{(A7)}$$

where

$$g(z)=-\frac{\Omega r^*}{2}\sqrt{\frac{m}{2T}}\left[(1+\ln\cos\alpha)+\frac{\xi}{r^*}\right]$$

Figure 14 presents the function $\varepsilon(g)$.

Acknowledgments. The authors would like to thank the NASA Marshall Space Flight Center for support during the completion of this work.

Janet Luhmann thanks William J. Burke, David N. Walker, and another referee for their assistance in evaluating this paper.

References

Khazanov, G. V., N. H. Stone, E. N. Krivorutsky, and M. W. Liemohn, Current-produced magnetic field effects on current collection, *J. Geophys. Res.*, *105*, 15,835, 2000.

Laframboise J. G., Theory of spherical and cylindrical Langmuir probes in collisionless Maxwellian plasma at rest, *Rep. 100*, Univ. of Toronto, Inst. of Aerosp. Stud., Toronto, Ont., Canada, 1966.

Laframboise, J. G., and J. Rubinstein, Theory of a cylindrical probe in a collisionless magnetoplasma, *Phys. Fluids*, *19*, 1900, 1976.

Press, W. H., S. A. Teukolsky, W. T. Vetterling, and B. P. Flannery, *Numerical Recipes in FORTRAN,* Cambridge Univ. Press, New York, 1986.

Sanmartin, J. R., and R. D. Estes, The orbital motion limited regime for cylindrical Langmuir probes, *Phys. Plasmas, 6,* 395, 1999.

Sanmartin, J. R., M. Martinez-Sanchez, and E. Ahedo, Bare wire anodes for electrodynamic tethers, *J. Propuls. Power*, *9*, 353, 1993.

Szuszczewicz, E. P., and P. Z. Takacs, Magnetosheath effects on cylindrical Langmuir probes, *Phys. Fluids*, *22*, 2424, 1979.

G. V. Gamayunov, G. V. Khazanov, and E. N. Krivorutsky, Geophysical Institute, University of Alaska Fairbanks, 903 Koyukuk Drive, P. O. Box 757320, Fairbanks, AK 99775-7320. (khazanov@gi.alaska.edu)

M. W. Liemohn, Space Physics Research Laboratory, University of Michigan, Ann Arbor, MI 48109-2143. (liemohn@umich.edu)

N. H. Stone, Space Sciences Laboratory, NASA Marshall Space Flight Center, Huntsville, AL 35812.

(Received September 8, 2000; revised December 4, 2000; accepted January 4, 2001.)